NO2 adsorption mechanism on TiO2: An in-situ transmission infrared spectroscopy study

L. Sivachandiran, F. Thevenet, Antoine Rousseau, D. Bianchi

NO_2 adsorption mechanism on TiO_2: an *In-Situ* transmission infrared spectroscopy study

L. Sivachandiran[a,b,c*] sivachandiran.loganathan@univ-orleans.fr, F. Thevenet[a,2], A. Rousseau[c], D. Bianchi[d]

[a] Mines Douai, SAGE, F-59508, Douai, France.

[b] Université de Lille, F-59000, Lille, France

[c] Laboratoire de Physique des Plasmas, École Polytechnique, UPMC, Université Paris Sud 11, CNRS Palaiseau, France.

[d] IRCELYON Université Claude Bernard Lyon 1, Bat Chevreul, UMR CNRS 5658, F-69100 Villeurbanne, France.

* Corresponding author at: GREMI, CNRS-Université d'Orléans, 45067 Orléans, France. Tel: +33 (0)2 38 49 43 85; fax: + 33 (0)2 38 41 71 54.

Graphysical abstract

Research Highlights

- As soon as NO_2 molecules reach TiO_2 surface, they dimerized to N_2O_4.
- The adsorbed N_2O_4 undergoes intra and intermolecular disproportionation reactions.

- Intramolecular reaction, within N_2O_4, produces m-NO_3^- $_{(ads)}$ and NO^+ $_{(ads)}$.
- Intermolecular reaction, between NO_2^- and N_2O_4, produces b-NO_3^- $_{(ads)}$ and NO $_{(g)}$.
- Strongly adsorbed b-NO_3^- species poisons and decreases the NO_2 storage capacity.

Abstract

The adsorption of NO_2 on oxidized TiO_2 surface, under dark condition at 296 K, has been investigated by *in-situ* transmission Fourier Transform Infrared Spectroscopy (trans-FTIR) as a function of time. It enabled the determination of detailed NO_2 reactive adsorption mechanisms on TiO_2. It was evidenced that, as soon as NO_2 molecules adsorb on TiO_2 surface it dimerize to adsorbed N_2O_4 species. The strongly adsorbed N_2O_4 undergoes intramolecular disproportionation reaction and produces: (i) weakly adsorbed monodentate nitrate (m-NO_3^-) species and, (ii) highly reactive NO^+ and/or N_2O_3 species on Ti^{4+} sites and O^{2-} sites, respectively. The NO^+ species reacts with surface lattice oxygen (O^{2-}) and produces more stable NO_2^- on Ti^{4+} sites. Then, the NO_2^- undergoes intermolecular disproportionation reaction with another strongly adsorbed N_2O_4 molecule and produces strongly adsorbed bidentate nitrate (b-NO_3^-) species on Ti^{4+} sites and releases NO in the gas phase. It was also noticed that, as adsorption time increases, the weakly adsorbed m-NO_3^- species are converted into strongly adsorbed b-NO_3^- species. The intramolecular disproportionation reaction rate depends on NO_2 partial pressure, whereas the intermolecular disproportionation reaction rate depends on the coverage of NO_2^- species and the number of available Ti^{4+} sites. This mechanism is assessed for different NO_2 partial pressures ranging from 25 to 100 Pa. This study reveals that the configuration and the amount of the N-containing species on activated TiO_2 surface depend on the NO_2 concentration and the contact time.

Keywords: TiO_2, NO_2, Adsorption, monodentate NO_3^-, bidentate NO_3^-

1. Introduction

Tropospheric Emission Monitoring Internet Service (TEMIS) [1] reports that most of the NO_2 emission originates from the European Union and China. The U.S. Environmental Protection Agency (EPA) regulates only nitrogen dioxide (NO_2) as a surrogate for NO_X, because it is the most prevalent form of NO_X in the atmosphere generated by anthropogenic activities [2]. NO_2 is not only an important air pollutant by itself, but it is also a key reactant in the atmosphere to form ozone (O_3) through series of reactions with volatile organic compounds (VOCs) [3] and acid rain.

NO_2 is produced in combustion processes under lean, i.e. oxygen-rich conditions. Emerging technologies favor the formation of NO_2 instead of NO during the combustion of fuels because the high reactivity of NO_2 makes easier subsequent DeNOx operations [4,5]. In $DeNO_X$ process, owing to its acidic property, thermal and mechanical stability, γ-Al_2O_3 is a widely used support [6]. However, new support materials are also studied either in their pure form or in mixture with other metal-oxides [7]. In this regards TiO_2 has been intensively studied due to its better sulfur tolerance [8] and controlled surface dispersion of barium oxide (BaO) [9] as compared to γ-Al_2O_3.

In particular, the most important step in $DeNO_X$ process is the adsorption of NO_2 on supporting materials. In spite of stability, NO_2 molecule strongly adsorbs on metal centers due to high electron affinity [10] (2.3 eV). It is demonstrated that metal oxides are very efficient as sorbents or catalysts for trapping and/or converting NO_2 and other NO_X species [11,12,13,14]. It is reported that depending on the NO_X concentration and adsorption time, there may be variation in thermal regeneration temperature and time [15]. Therefore, it is necessary to understand the nature of the adsorbed species on metal oxide surface to optimize the NO_X removal process.

Ramis et al. examined the NO_2 adsorption on TiO_2 surface at room temperature and evidenced that NO_2 adsorbs on Ti^{4+} sites through O, N, or a combination of both [16,17]. Hadjiivanov et al. [18] and Dalton et al. [19] demonstrated the NO_2 adsorption on anatase surface and showed that isolated OH-groups on TiO_2 surface react with NO_2 to produce adsorbed NO_3^- and water, on TiO_2 surface, and NO in the gas phase. In addition, authors have also reported that α and β- Lewis sites on TiO_2 surface respectively produce mono and bidentate NO_3^- species. This work is not in complete agreement with other approaches based on accurate gas phase analyses [15]. Indeed, Sivachandiran et al. [15] evidenced that,

under dark condition, the nature of species adsorbed on TiO_2 surface highly depends on: (i) the NO_2 concentration and (ii) the duration of adsorption. The proposed mechanism by Sivachandiran et al [15] is summarized in Eq. 1 to Eq. 3.

$$2NO_{2\,(ads)} \leftrightarrow NO_{3\,(ads)}^{-} + NO^{+}{}_{(ads)} \qquad Eq.1$$

$$NO^{+}{}_{(ads)} + O^{2-}\left(TiO_{2\,surface\,lattice}\right) \leftrightarrow NO_{2\,(ads)}^{-} \qquad Eq.2$$

$$Surface\,coverage\left(NO_{2\,(ads)}^{-} + NO_{3\,(ads)}^{-}\right) > 0.2\,then:$$

$$NO_{2\,(ads)}^{-} + NO_{2\,(ads)} \leftrightarrow NO_{3\,(ads)}^{-} + NO_{(g)} \qquad Eq.3$$

Therefore, the global NO_2 adsorption stoichiometry equation can be written by summing up Eq. 1 to Eq. 3 as denoted in Eq. 4:

$$3NO_{2\,(ads)} + O^{2-}(TiO_{2\,surface\,lattice}) \leftrightarrow 2NO_{3\,(ads)}^{-} + NO_{(g)} \qquad Eq.4$$

According to Eq. 4, three NO_2 molecules are involved to produce one NO in the gas phase and two NO_3^- species adsorbed on TiO_2 surface. In one hand, as reported in Eq. 1, the first NO_3^- species is produced by disproportionation reaction between two adsorbed NO_2 species. Then, as reported in Eq. 3, the second NO_3^- is produced by disproportionation reaction between the produced intermediate species NO_2^- and the molecularly adsorbed NO_2. Thus, it can be proposed that, these two NO_3^- species could be different regarding their adsorption modes. Indeed, it was noticed that [15], during temperature programmed desorption (TPD), the adsorbed NO_3^- species are desorbed in two distinct peaks. These findings means that, the desorption energies of NO_3^- species produced in the Eq. 1 and in Eq. 3 are different. In addition to that, with increasing the adsorption time, the first NO_3^- desorption peak disappears. Thus, it can be suggested that, as the time progress the weakly adsorbed NO_3^- is converted into strongly adsorbed NO_3^- species. To assess these hypotheses and to follow the evolution of other adsorbed species, it is necessary to monitor the TiO_2 surface directly and continuously.

In this study, NO_2 adsorption mechanism has been investigated on TiO_2 surface, under dark condition at 296 K. The *in-situ* Transmission Fourier Transform Infrared Spectroscopy (trans-FTIR) was used to investigate the adsorbed species on TiO_2 surface before and after NO_2 adsorption experiments. The evolution of adsorbed species on TiO_2 surface is continuously monitored for various NO_2 partial

pressures like 25 and 100 Pa as a function of time in order to propose new insights regarding reactive adsorption mechanism of NO_2 on TiO_2.

2. Experimental description

Fig. 1 gives a general overview of the experimental and analytical setup. This experimental setup is adapted from the setup used and reported by Arsac et al. [20] for photocatalytic studies. In brief, the main body of the reactor consists of a Pyrex tube characterized by 40 mm of outer diameter, 35 mm of inner diameter and 2.5 mm of wall thickness. As shown in Fig. 1, four different parts can be distinguished in this experimental setup: (1) Gas stream preparation and pumping, (2) Furnace for thermal pretreatment, (3) trans-FTIR, and (4) TiO_2 sample holder.

2.1. TiO_2 sample preparation, gas stream introduction

The TiO_2 sample is prepared by compressing 70 mg of TiO_2-P25 Degussa powder with 5 x 10^4 Pa pressure. The obtained pellet is a disc of 18 mm diameter. Then the sample is placed inside the quartz sample holder (4), Fig. 1, by removing the part (2). As presented in insert part (4) of Fig. 1, the length of the sample holder is 150 mm. One end of the sample holder is connected to the magnetic movement system using tungsten wire, while the other end is specially designed with a round shape of 19 mm inner diameter to hold the TiO_2 disc. The reactor is pumped down by opening the valve V_2 connected to a vacuum pump. Thus, a minimum total pressure of 0.5 Pa can be reached in the reactor.

The valves V_3 and V_4 are respectively used to introduce 1% NO_2/He, and pure O_2. The total volume of the reactor has been evaluated by volumetric method using the buffer volume connected through the valve V_5. The determined volume is 2 ± 0.1 L. Before adsorption, it is necessary to purge the valves and the upstream pipe lines connected to the gas cylinders to avoid the TiO_2 sample contamination. The valve V_1 is used to isolate the part (1) from other parts of the reactor, and vacuum pump is used to purge the sample port valves (V_3, V_4) and the upstream line.

2.2. TiO_2 thermal pretreatment

As can be seen in Fig. 1, the part (2) is made of quartz tube and covered with a removable furnace (Winkler, WRW00110). The furnace is used for sample pretreatment performed before any experiment. The sample temperature can be increased to 700 K and the temperature is monitored using

K-type thermocouple placed inside the furnace. On the top of the part (2), a magnetic sample movement system is connected and used to move the quartz sample holder (4), from part (2) to part (3). The sample is carefully moved to the heating part (2). Before thermal treatment the reactor is pumped down to 0.5 Pa total pressure by opening the valve V_2. Then, valve V_2 is closed and 2 x 10^4 Pa of pure O_2 are introduced into the reactor by opening the valve V_4. Once the pressure reaches the equilibrium, the sample temperature is linearly increased from 296 to 700 K with the heating rate of 1.1 $K.s^{-1}$. After 1 h of heating, the reactor is pumped down to 0.5 Pa, again 2 x 10^4 Pa of pure O_2 are introduced. After 2 h of thermal treatment, the furnace is switched off, the reactor is pumped down to 0.5 Pa and the sample is allowed to cool down to 296 K.

2.3. Analytical device: trans-FTIR

In part (3), transmission FTIR cell, so-called trans-FTIR (Brucker IFS-28), is used to characterize species adsorbed on TiO_2 sample. The sample surface is characterized before each step of the process. As shown in Fig. 1, the homemade IR cell consists in a Pyrex tube. Both ends of the tube are closed with CaF_2 windows characterized by 35 mm diameter and 3 mm thickness. This configuration leads to 80 mm optical path length. Viton O-rings are used to assemble tightly all parts of the IR cell. Further, a Pyrex tube is used to connect the IR cell to the other parts of the reactor. In addition to that, an appropriate system inserted inside the Pyrex tube is used to keep the TiO_2 sample in the same position, perpendicular to the IR beam, for all experiments. Finally, the transmitted IR radiations are recorded by DTGS detector at room temperature. The TiO_2 sample is continuously scanned from 4000 to 1100 cm^{-1}. FTIR spectra are collected and analyzed using OMNIC software with 5 scans per spectrum and 4 cm^{-1} spectral resolution.

2.4. NO_2 adsorption experiments

The NO_2 adsorption on TiO_2 surface has been investigated for two different partial pressures**:** 25 ± 2.5 and 100 ± 2.5 Pa. The pressure was monitored using vacuum gauge supplied by Cole-Parmer (EW-07379-22). For NO_2 adsorption experiment, the NO_2 cylinder is connected to the setup through the valve V_3. All the calibrated gas cylinders are provided by Air liquid. During the adsorption experiments, the TiO_2 sample is kept in the trans-FTIR cell and the surface is continuously scanned and the adsorbed species are monitored as a function of time.

3. Results and discussion

3.1. Thermally treated TiO_2 surface characterization before NO_2 adsorption

Fig. 2 shows the FTIR spectrum of TiO_2 surface after the thermal treatment and prior to any NO_2 adsorption. After thermal pretreatment, performed under pure O_2, the sample has been cooled to 296 K. The gas phase spectrum collected under 0.5 Pa of pure O_2 is used as background spectrum. As can be seen in Fig. 2, FTIR spectrum reveals four main IR bands at 3725, 3685, 3672 and 3640 cm^{-1}. The bands at 3725 and 3685 cm^{-1} are ascribed to isolated OH groups, and bands at 3672 and 3640 cm^{-1} are assigned to bridged hydroxyl groups [20,21,22,23]. The multiplicity of the hydroxyl groups on TiO_2-P25 sample is attributed to the presence of variety of Ti^{4+} sites on surface [23].

3.2. Temporal profiles of NO_2 adsorption on TiO_2 under dark condition

For adsorption, 25 x 10^2 Pa of 1% NO_2 in He, i.e. 25 Pa of NO_2 partial pressure, are introduced into the reactor. Fig. 3 shows the FTIR spectra of TiO_2 exposed to NO_2 for different durations. The assignment of the absorption bands of adsorbed species on TiO_2 surface is given in Table 1 [16, 17,18,24,25,26,27].

The introduction of NO_2 onto the TiO_2 sample, leads to the formation of several adsorbed NO_X species with absorption bands between 1100 and 2000 cm^{-1}. After 1 min of adsorption, strong absorption bands of ν(NO) are observed at 1708 and 1273 cm^{-1} with a weak ν(NO) band at 1360 cm^{-1}. These bands are assigned to the adsorbed N_2O_4 species [17,18]. In parallel, two well resolved ν(NO) bands attributed to monodentate nitrate (m-NO_3^-) species are observed at 1542 and 1243 cm^{-1} [16,17]. Meanwhile, ν(NO) absorption bands are observed at 1608, 1582, and 1288 cm^{-1}. These bands are ascribed to the bidentate nitrate (b-NO_3^-) species on TiO_2 surface [25,26]. In addition, two well resolved bands at 1628 and 1171 cm^{-1} are observed. These bands are assigned to the bridged nitrate species [27]. Notably, the intensities of the bands at 1542 and 1243 cm^{-1} (m-NO_3^-) and 1628 and 1171 cm^{-1} (bridged NO_3^-) decrease with increasing adsorption time. More importantly, after 20 min of adsorption, these bands disappear and the intensities of the bands at 1608, 1582 and 1288 cm^{-1} corresponding to b-NO_3^- species increase as adsorption progress. Thus, it can be suggested that, bridged and m-NO_3^- species are formed as intermediate species on TiO_2 surface, which are evidently converted into strongly adsorbed b-NO_3^- species.

In literature, Ramis et al. [16] reported that, on activated TiO_2 (723 K), the molecularly adsorbed NO_2 shows two well resolved characteristic bands at 1617 and 1320 cm^{-1}. Interestingly, as reported in Fig. 3, these two bands are not observed. Therefore, it can be suggested that, on oxidized TiO_2 surface, at room temperature, as soon as NO_2 molecules adsorb, they get dimerized into strongly adsorbed N_2O_4 [18]. Meanwhile, along with N_2O_4 species, weak broad ν(NO) bands at 1914 cm^{-1} and at 1858 cm^{-1} are also observed, and these bands disappear after 20 min of adsorption. These bands can be assigned to the adsorbed NO^+ species on TiO_2 surface [28,17]. Similarly, after 4 min of adsorption, a weak ν(NO) band at 1222 cm^{-1} is observed, and it disappears after 40 min of adsorption. This band can be assigned to the weakly adsorbed NO_2^- species on TiO_2 surface [18].

It is worth to mention that the adsorbed N_2O_3 species on TiO_2 surface exhibit absorption bands between 1930 and 1880 cm^{-1} [29], therefore it is very difficult to differentiate between the adsorbed N_2O_3 and the adsorbed NO^+ species on TiO_2 surface. However, Mikhaylov et al. [30] observed N_2O_3 species on TiO_2 surface only during NO and O_2 adsorption studies by the reaction between NO and NO_2 species on TiO_2 surface and also suggested that it is hard to identify the N_2O_3 species during NO_2 adsorption experiments. Ito et al. [31] suggested that during NO adsorption, N_2O_3 species exist in equilibrium with NO_2^- and NO^+ species on CeO_2 surface as denoted in Eq. 5. In addition, Sentürk et al. [32] demonstrated NO_2 adsorption on TiO_2/Al_2O_3 binary mixture and suggested that NO^+ and NO_2^- species are produced on the surface from N_2O_3 species as reported in Eq. 5. Therefore, it can be proposed that the existence of N_2O_3 could be correlated to the formation on NO^+ species on TiO_2 surface. Moreover, the consumption of NO^+ and NO_2^- decreases the N_2O_3 concentration on TiO_2 surface at room temperature.

$$N_2O_{3(ads)} \leftrightarrow NO^+ + NO^-_{2(ads)} \qquad \text{Eq. 5.}$$

3.3. NO_2 adsorption mechanism proposal based on surface analysis

The integration of characteristic absorption bands of adsorbed species leads to follow their individual evolutions as a function of time. For all species, the normalized absorbance is calculated by considering their individual maximum absorbance as 1. The normalized absorbances of primarily produced species N_2O_4 is reported in Fig. 4 (a) and NO^+ and m-NO_3^- species are reported in Fig. 4 (b). Similarly, the normalized absorbances the intermediate species NO_2^- and the strongly adsorbed b-NO_3^- species are reported in Fig. 4 (c). The N_2O_4 absorbance is followed through ν(NO) stretching band at 1708 cm^{-1}, and the adsorbed NO^+ is followed through ν(NO) band at 1914 cm^{-1}. The m-NO_3^- is followed

through ν(NO) band at 1542 cm^{-1}, and the b-NO_3^- is followed through ν(NO) band at 1582 cm^{-1}. The NO_2^- is followed through ν(NO) band at 1222 cm^{-1}.

As can be seen in Fig. 4 (a), the absorbance of N_2O_4 reaches maximum within 3 min, then steeply decreases to zero within 70 min of adsorption. Meanwhile, as reported in Fig. 4(b), the absorbance of NO^+ species increases and reaches maximum at 8 min, then decreases with increasing the adsorption time. The NO^+ species on TiO_2 surface is produced by intramolecular disproportionation reaction in N_2O_4 species at room temperature. The temporal profiles of N_2O_4 and NO^+ species show that they are converted into other species along adsorption experiment. The identification of NO^+ species on TiO_2 surface and subsequent conversion are coherent with the mechanism previously suggested by Sivachandiran et al [15]. Our observations confirm this hypothesis.

Several experimental [33,34] and numerical studies [35,36,37] revealed the symmetric O_2N-NO_2 and asymmetric ONO-NO_2 isomers of N_2O_4. Fateley et al. [38] first reported the asymmetric isomer of N_2O_4 and demonstrated that it converts into an ion-pair of $NO^+NO_3^-$ at ambient temperature. Colussi et al. [39] estimated the heat of formation of ONO-NO_2 isomer from experiment to be 6.7 ± 1 kcal/mol which is only 4.5 kcal/mol less than the symmetry O_2N-NO_2 isomer. Givan et al. [33] evidenced that, using FTIR and Raman spectroscopy techniques, in spite of the fact that ONO-NO_2 is less stable, it is the main source of nitrosonium nitrate, i.e. $NO^+NO_3^-$ formation on copper substrate. Therefore, it can be suggested that on TiO_2 surface the N_2O_4 is adsorbed in the asymmetric form and produces NO^+ and NO_3^- on TiO_2 surface. The N_2O_4 formation on TiO_2 surface and subsequent NO^+ formation on TiO_2 lattice and m-NO_3^- species production are summarized in Eq. 6 and Eq. 7.

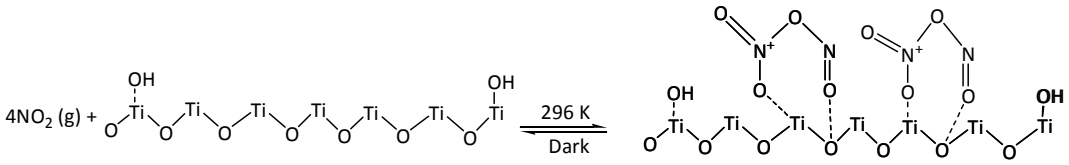

Eq. 6

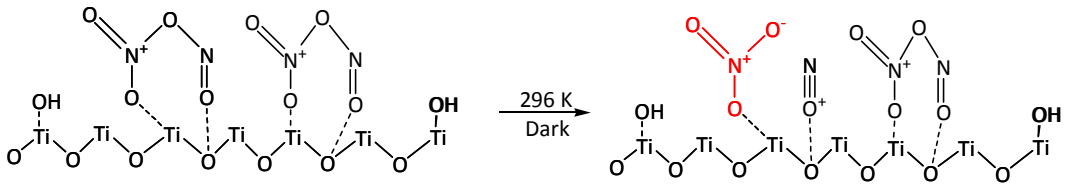

Eq. 7

As reported in Fig. 4 (b), m-NO_3^- reaches maximum within 20 min, then gradually decreases with time. Thus, the decrease in intensity of m-NO_3^- species shows that it is slowly converted into other

species. We suggest that this species is converted into the strongly adsorbed b-NO_3^- species, since this is the only species observed beyond 70 min of adsorption. This hypothesis is further praised by the increase in intensity of the strongly adsorbed b-NO_3^- species as reported in Fig. 4 (c). Moreover, the decrease in intensity of m-NO_3^- is in accordance with the results reported by Sivachandiran et al. [15] based on gas phase analysis carried out at the reactor downstream. Indeed, it is possible to correlate the amount of NO_2 desorbed during TPD as a first peak to weakly adsorbed m-NO_3^- species. Therefore, it can be concluded that, the m-NO_3^- species are produced by the intramolecular disproportionation reaction from N_2O_4 species. Meanwhile, the relatively less stable NO^+ species adsorbed on TiO_2 surface reacts with the lattice O^{2-} and produces NO_2^- species. The m-NO_3^- slow conversion and NO_2^- species production can be summarized as follows:

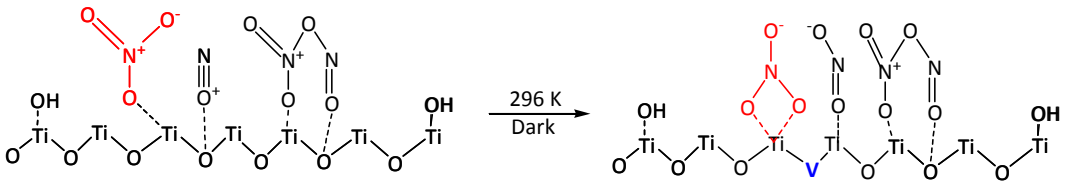

Eq. 8

As reported in Fig. 4(c), similarly to m-NO_3^- species, NO_2^- reaches maximum at 20 min, then steeply decreases to zero within 70 min of adsorption. It can be suggested that the NO_2^- species reacts with the adsorbed ONO-NO_2 and produces the strongly adsorbed b-NO_3^- species as reported in Eq. 9. The NO_2^- formation rate on TiO_2 surface is lower than the NO^+ and ONO-NO_2 formation rates, subsequently, it can be suggested that, NO_2^- is produced as an intermediate species. As demonstrated by Apostolescu et al. [40] on Al_2O_3 surface, and as suggested by Sivachandiran et al. [15], and Mikhaylov et al. [30] on TiO_2 surface, it can be concluded that NO_2^- is produced from NO^+ species. At room temperature, NO^+ is relatively unstable therefore, it may react with O^{2-} on TiO_2 surface lattice leading to NO_2^- species [40] and Ti^{3+} sites on TiO_2 surface [41].

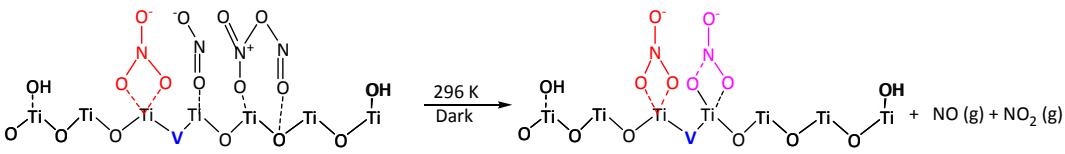

Eq. 9

These findings give the possibility to complete and detail the mechanisms reported by Sivachandiran et al [15]. The detailed complete global NO_2 adsorption equation can be written by summing up Eq. 6 to Eq. 9 as denoted in Eq. 10.

$$4NO_{2\,(ads)} + O^{2-}\left(TiO_{2\ \text{surface lattice}}\right) \overset{296\ K(dark)}{\leftrightarrow} 2\ b-NO^{-}_{3(ads)} + NO_{(g)} + NO_{2(g)} \qquad \text{Eq. 10}$$

In Eq. 8 and Eq. 9, "[V]" represents the lattice vacancy generated by the consumption of O^{2-} by NO^{+} species at 296 K. As denoted in Eq. 8, NO and NO_2 have not been observed in the gas phase using *In-Situ* trans-FTIR. Although NO possess a strong polarization, it is a linear molecule with low extinction coefficient, thus, it is not observed in the gas phase under our experimental conditions. It can be suggested the as soon as NO_2 released into the gas phase, it could get dimerized on TiO_2 surface with another NO_2 molecule released in similar reaction as reported in Eq. 10. However, as abovementioned, gas phase monitoring reported by Sivachandiran et al. [15] interestingly complements the trans-FTIR results.

3.4. Assessment of NO_2 adsorption mechanism for various partial pressures

The proposed NO_2 adsorption mechanism on TiO_2 has been assessed for two different NO_2 partial pressures: 25 and 100 Pa. The temporal evolutions of adsorbed species on TiO_2 surface are discussed in the following.

3.4.1. Formation of N_2O_4

Fig. 5 shows the evolution of adsorbed N_2O_4 species on TiO_2 surface as a function of time. For each investigated partial pressure the adsorbed N_2O_4 species have been observed as soon as NO_2 is introduced into the reactor. Therefore, it can be concluded that the N_2O_4 formation process on TiO_2 surface does not depend on NO_2 partial pressure. However, as can be seen in Fig. 5, the temporal evolution of N_2O_4 varies with NO_2 partial pressures. It can be expected that the increase in NO_2 partial pressure could increase the multilayer adsorption of N_2O_4 on TiO_2 surface. Nevertheless, the time required to reach the maximum of N_2O_4 on TiO_2 surface increases with increasing NO_2 partial pressure. Unlike 25 Pa, for 100 Pa partial pressures, the maximum is reached after 25 min adsorption, and then absorbance gradually decreases with time. This finding suggests the fact that, the increase in NO_2 partial pressure favors N_2O_4 conversion into m-NO_3^- and NO^+ species on TiO_2 surface as reported in Eq. 6. Moreover, for 100 Pa, even after 70 min of adsorption, more than 70% of adsorbed N_2O_4 species remain

on TiO_2 surface. This observation implies the fact that increase in NO_2 partial pressure increases the concentration of adsorbed N_2O_4 species and are not completely converted into other adsorbed species. These suggestions could be confirmed by monitoring the evolution of m-NO_3^- and NO^+ on TiO_2 surface for various NO_2 partial pressures.

3.4.2. Intramolecular disproportionation reaction: Formation of m-NO_3^- and NO^+ species

Fig. 6 reports the normalized absorbances of (a) m-NO_3^- and (b) NO^+ species produced by the intramolecular disproportionation reaction in N_2O_4 species as a function of time for 25 and 100 Pa. It is worth to mention that for each investigated NO_2 pressure, the temporal profiles of m-NO_3^- and NO^+ follow the same pattern.

As reported in Fig. 6 (a), unlike N_2O_4 (Fig. 5) for both 25 and 100 Pa partial pressure the maxima of m-NO_3^- are reached at 20 min. Indeed, as adsorption progresses, for 25 Pa pressure the m-NO_3^- species concentration gradually decreases and about 70% remain even after 70 min, whereas, for 100 Pa it rapidly decreases with time and only about 10% remain after 70 min of adsorption. As suggested in *section 3.3*, the decrease in m-NO_3^- coverage could be correlated to the formation of b-NO_3^-. As reported by Hadjiivanov et al. [18], even though the m-NO_3^- species are produced from the adsorption of N_2O_4 on β-Lewis sites, i.e. Ti^{4+} sites with one oxygen vacancy, the relatively less stable m-NO_3^- has been converted into stable b-NO_3^- species. Indeed, it can be suggested that the amount of m-NO_3^- is mainly influenced by the first intramolecular disproportionation reaction and free adsorption sites on TiO_2 surface. This finding suggests the fact that the increase in NO_2 partial pressure favors the rate of m-NO_3^- conversion into b-NO_3^- species on TiO_2 surface.

As reported in Fig. 6 (b), unlike m-NO_3^- species, the time required to reach maximum coverage of NO^+ on TiO_2 surface increases with increasing the NO_2 partial pressure. Nevertheless, the rate of NO^+ conversion decreases with increasing the NO_2 partial pressure. For instance, for 25 Pa the maximum NO^+ concentration is reached at 5 min, whereas for 100 Pa the maximum reaches at 20 min. This finding, similarly to N_2O_4 formation, emphasizes the fact that the increase in NO_2 partial pressure increases the formation and conversion of NO^+ on TiO_2 surface for the first few minutes of adsorption. And thereafter, all these reactions are mainly dependent on the available free adsorption sites on TiO_2 surface. Although the adsorbed NO^+ species are relatively less stable on TiO_2 surface, for 100 Pa pressure, after 70 min adsorption, more than 80% remain on the surface. The existence of NO^+ can be ascribed to the

formation of N_2O_3 by reacting with NO_2^- on TiO_2 surface as reported in Eq. 5. This finding highlights the fact that NO^+ conversion into NO_2^- is dependent on the surface coverage of m-NO_3^- and b-NO_3^- species, under dark condition.

3.4.3. Formation of NO_2^-: Consumption of TiO_2 surface lattice oxygen (O^{2-})

As discussed in *section 3.3*, the evolution of NO_2^- species is followed as a function of time for each NO_2 partial pressure and reported in Fig. 7. The intermediate NO_2^- is produced by the reaction between NO^+ and TiO_2 lattice oxygen (O^{2-}).

As can be seen in Fig. 7, similarly to m-NO_3^- and NO^+ (Fig. 6), the coverage of NO_2^- also varies according to the NO_2 partial pressure. For both 25 and 100 Pa partial pressure, the maxima are reached at 15 min. As reported in Eq. 8, though the NO_2^- is produced form the adsorbed NO^+ and/or N_2O_3 species, the rate of NO_2^- formation is not only dependent on NO^+ but also controlled by the intermolecular disproportionation reaction as reported in Eq. 12. As noticed in Fig. 7, after reaching the maximum coverage, for 100 Pa NO_2 partial pressure, the NO_2^- concentration decreases faster than that of 25 Pa, and it reaches zero after 50 min of adsorption. Interestingly, as reported in Fig. 6 (b), at 50 min of adsorption, the NO^+ coverage is about 90%. This finding emphasizes the fact that NO^+ conversion is not dependent on the NO_2^- coverage on TiO_2 surface. Furthermore, as denoted in Eq. 8 and Eq. 11, it can be suggested that the rate of NO^+ conversion, i.e. the reaction between NO^+ and the lattice oxygen (O^{2-}) is much slower than the NO_2^- conversion into b-NO_3^- species.

$$NO^+_{(ads)} \leftrightarrow O^{2-}_{(\text{surface lattice})} \overset{\text{slow}}{\leftrightarrow} NO^-_{2\,(ads)} \qquad \text{Eq.11}$$

$$NO^-_{2\,(ads)} \leftrightarrow N_2O_{4\,(ads)} \overset{\text{fast}}{\leftrightarrow} b-NO^-_{3\,(ads)} + NO_{(gas)} + NO_{2(gas)} \qquad \text{Eq.12}$$

3.4.4. Intermolecular disproportionation reaction: formation of b-NO_3^-

As reported in Fig. 3, it is evidenced that the b-NO_3- are the strongly adsorbed species on TiO_2 surface produced through intermolecular disproportionation reaction between NO_2^- and N_2O_4 species on TiO_2 surface. Therefore, it can be proposed that the increase in NO_2 partial pressure could presumably

increase the rate of b-NO_3^- formation on TiO_2 surface. The evolution of b-NO_3^- absorbance for 25 and 100 Pa NO_2 partial pressure, as function of time, is reported in Fig. 8.

As can be noticed in Fig. 8, for 25 and 100 Pa, the b-NO_3^- absorbances follow the same trend. However, as expected, the rate of b-NO_3^- formation increases with increasing the NO_2 partial pressure. Indeed, for 25 Pa partial pressure, the b-NO_3^- absorbance gradually increases until 70 min of adsorption. Whereas, for 100 Pa the maximum absorbance is reached at 50 min. Interestingly, for 100 Pa NO_2 partial pressure, as reported in Fig. 6 (b) and Fig. 7, after 50 min of adsorption the coverage of m-NO_3^- and NO_2^- reach 10% and zero, respectively. Therefore, there is no further intermolecular disproportionation reaction to produce b-NO_3^- species. This finding shows that, the b-NO_3^- species are produced by intermolecular disproportionation reaction and slow conversion of m-NO_3^- species. Moreover, the rate of the reaction is dependent on NO_2 partial pressure and available free sites on TiO_2 surface.

As reviewed by Roy and Baiker [42], the storage of nitrate species on supports, i.e. metal oxide or mixture of metal oxides, is the main step directly linked with NO_X reduction to N_2. As reported by Sivachandiran et al. [15], under a constant operating condition, an increase in NO_2 concentration decreases the NO_2 storage capacity. By taking into account the species monitored using gas phase FTIR, at the reactor downstream, it was suggested that the strongly adsorbed NO_3^- species decreases the NO_2 adsorption/storage on TiO_2 surface. In this study using trans-FTIR, it is evidenced that the strongly adsorbed b-NO_3^- species prevents the intra and intermolecular disproportionation reactions. As a result the adsorbed b-NO_3^- species poisons the TiO_2 surface toward NO_2 adsorption and decreases the NO_X storage capacity.

4. Conclusions

At 296 K, under dark condition, 25 and 100 Pa of NO_2 in He are introduced, and the adsorbed species on TiO_2 surface are followed using *In-Situ* trans-FTIR spectroscopy, as a function of time. The main conclusions of this study are summarized below.

1. As soon as NO_2 is introduced onto TiO_2 surface, within less than 1 min, NO_2 species are dimerized to produce N_2O_4 on TiO_2 surface.

2. The species identified on TiO_2 surface are in accordance with the species proposed from the gas phase analysis performed at the reactor downstream as demonstrated by Sivachandiran et all [15].

3. It was evidenced that, the first disproportionation reaction proceeds via an intramolecular disproportionation reaction, i.e. within one adsorbed N_2O_4 species, and produces weakly adsorbed monodentate nitrate (m-NO_3^-) species and highly reactive NO^+ species on TiO_2 surface. It was observed that, with time, the weakly adsorbed m-NO_3^- species have been converted into strongly adsorbed bidentate nitrate (b-NO_3^-) species. Meanwhile, the highly active NO^+ species reacts with the lattice oxygen (O^{2-}) and produces NO_2^- on TiO_2 surface.

4. The second disproportionation reaction is an intermolecular reaction, i.e. reaction between N_2O_4 and NO_2^- species on TiO_2 surface. This reaction depends on the coverage of NO_2^- and N_2O_4 species. It is proposed that, these two species should be in close vicinity to induce the disproportionation reaction and to produce NO in the gas phase and the strongly adsorbed b-NO_3^- species on TiO_2 surface.

5. It was demonstrated that the rate of N_2O_4, m-NO_3^- and NO^+ species formation are dependent on the NO_2 partial pressure.

6. The intermolecular disproportionation reaction, i.e. the reaction between NO_2^- and N_2O_4 is faster than the relatively less stable NO^+ conversion into NO_2^- species.

7. The NO_2 adsorption mechanism proposed based on gas phase analysis performed at the reactor downstream [15] is confirmed and precisely followed by *In-Situ* TiO_2 surface analyses.

Acknowledgements

The authors greatly acknowledge the French National Research Agency (ANR) for its financial support. Experiments have been performed in the framework of the ANR Blanc-RAMPE project.

References

[1] Environmental Health Perspectives. 116-8 (2008) A338.

[2] United States Environmental Protection Agency (EPA): http://www2.epa.gov/isa/integrated-science-assessment-isa-nitrogen-dioxide-health-criteria.

[3] J.H. Seinfeld, S.N. Pandis, Atmospheric Chemistry and Physics: from Air Pollution to Climate Change, 2nd ed, John Wiley: New York, 2006.

[4] M. Shimokawabe, K. Itoh, N. Takezawa, Catal. Today., 36 **(1997)** 65-70.

[5] M. Shimokawabe, A. Ohi, N. Takezawa, React. Kinet. Catal. Lett., 52 **(1994)** 393-397.

[6] D. Mei, Q. Ge, J.H. Kwak, D.H. Kim, J. Szanyi, C.H. Peden, J. Phys. Chem. C., 112 **(2008)** 18050-18060.

[7] N. Takahashi, A. Suda, I. Hachisuka, M. Sugiura, H. Sobukawa, H. Shinjoh, Appl. Catal. B. Environ., 72 **(2007)** 187-195.

[8] L. Li, Q. Shen, J. Cheng, Z. Hao, Catal. Today., 158 **(2010)** 361−369.

[9] S.M. Andonova, G.S. Şentürk, E. Özensoy, J. Phys. Chem. C., 114 **(2010)** 17003-17016.

[10] C. Morterra, G. Ghiotti, E. Garrone and E. Fisicaro, J. Chem. Soc. Faraday Trans 1., 76 **(1980)** 2101-2113.

[11] J. Haubrich, R. G. Quiller, L. Benz, Z. Liu, C. M. Friend, Langmuir., 26 **(2010)** 2445–2451.

[12] J.A. Rodriguez, T. Jirsak, G. Liu, J. Hrbek, J. Dvorak, A. Maiti, J. Am. Chem. Soc., 123 **(2001)** 9597-9605.

[13] J. Abad, O. Bohme, E. Roman, Langmuir., 23 **(2007)** 7583-7586.

[14] A. Folli, S.B. Campbell, J.A. Anderson, D.E. Macphee, J Photochem. Photobio A., 220 **(2011)** 85-93.

[15] L. Sivachandiran, F. Thevenet, P. Gravejat, A. Rousseau. Appl. Catal. B. Environ., 143 **(2013)** 196-204.

[16] G. Ramis, G. Busca, V. Lorenzelli, Appl. Catal., 64 **(1990)** 243-257.

[17] G. Ramis, G. Busca, F. Bregani, P. Forzatti, Appl. Catal., 64 **(1990)** 259-278.

[18] K. Hadjiivanov, V. Bushev, M. Kantcheva, D. Klissurski, Langmuir., 10 **(1994)** 464-471.

[19] J.S Dalton, P.A Janes, N.G Jones, J.A Nicholson, K.R Hallam, G.C Allen, Environ. Pollut., 120 **(2002)** 415-422.

[20] F. Arsac, D. Bianchi, J. M. Chovelon, C. Ferronato, J. M. Herrmann, J. Phys. Chem. A., 110 **(2006)** 4202-4212.

[21] P.F. Rossi, G. Busca, V. Lorenzelli, O. Saur, J.C. Lavalley, Langmuir., 3 **(1987)** 52-58.

[22] M.E. Maazawi, A.N. Finken, A.B. Nair, V.H. Grassian, J. Catal., 191 **(2000)** 138-146.

[23] C. Deiana, E. Fois, S. Coluccia, G. Martra, J. Phys. Chem. C., 114 **(2010)** 21531−21538.

[24] G. Piazzesi, M. Elsener, O. Krocher, A. Wokaun, Appl. Catal. B. Environ., 65 **(2006)** 169-174.

[25] K. Hadjiivanov, H. Knozinger, Phys. Chem. Chem. Phys., 2 **(2000)** 2803-2806.

[26] A.L. Goodman, E.T. Bernard, V.H. Grassian, J. Phys. Chem. A., 105 **(2001)** 6443-6457.

[27] G.M. Underwood, T.M. Miller, V.H. Grassian, J. Phys. Chem. A., 103 **(1999)** 6184-6190.

[28] R.V. Mikhaylov, A.A. Lisachenko, B.N. Shelimov, V.B. Kazansky, G. Martra, G. Alberto, S. Coluccia, J. Phys. Chem. C., 113 **(2009)** 20381-20387.

[29] K. Hadjiivanov, Identification of Neutral and Charged NxOy Surface Species by IR Spectroscopy. Catal. Rev.: Sci. Eng., 42 **(2000)** 71−144.

[30] R. V. Mikhaylov, A. A. Lisachenko, B. N. Shelimov, V. B. Kazansky, G. Martra, S. Coluccia, J. Phys. Chem. C., 117 **(2013)** 10345−10352.

[31] E. Ito, Y.J. Mergler, B.E. Nieuwenhuys, H. van Bekkum, C.M. van den Bleek, Microporous Materials., 4 **(1995)** 455-465.

[32] G. S. Sentürk, E. I. Vovk, V. I. Zaikovskii, Z. Saya, A. M. Soylu, V. I. Bukhtiyarov, E. Ozensoy, Catal. Today., 184 **(2012)** 54-71.

[33] A. Givan, A. Loewenschuss, J. Chem. Phys., 90 **(1989)** 6135.

[34] D.A. Pinnick, S. F. Agnew, B. I. Swanson, J. Phys. Chem., 96 **(1992)** 7092.

[35] W.G. Liu, W.A. Goddard, J. Am. Chem. Soc., 134 **(2012)** 12970−12978.

[36] M.L. McKee, J. Am. Chem. Soc., 117 **(1995)** 1629-1637.

[37] E. A. Pidko, P. Mignon, P. Geerlings, R.A. Schoonheydt, R.A. van Santen, J. Phys. Chem. C., 112 **(2008)** 5510-5519.

[38] W.G. Fateley, H.A. Bent, B. Crawford, J. Chem. Phys., 31 **(1959)** 204.

[39] A.J. Colussi, M.A. Grela, J. Phys. Chem., 97 **(1993)** 3775.

[40] N. Apostolescu, T. Schröder, S. Kureti, Appl. Catal. B. Environ., 51 **(2004)** 43-50.

[41] G.B. Hoflund, H.L. Yin, A.L. Grogan, D.A. Asbury, Langmuir., 4 **(1988)** 346-350.

[42] S. Roy, A. Baiker, Chem. Rev., 109 **(2009)** 4054-4091.

Figure caption

Fig. 1. General schematic of the experimental setup.

Fig. 2. FTIR spectrum of TiO_2 pellet recorded at 296 K after thermal pretreatment. TiO_2 sample was pretreated under $2x10^4$ Pa total pressure of pure O_2 at 700 K for 2 h.

Fig. 3. *In-Situ* trans-FTIR spectra of TiO_2 sample exposed to 25 Pa of NO_2 (1%/He) under dark condition at 296 K.

Fig. 4. Evolution of adsorbed species on TiO_2 surface during NO_2 adsorption. NO_2 adsorption is carried out at 296 K and under 25 Pa of NO_2 partial pressure. Normalized absorbances of adsorbed (a) N_2O_4, (b) NO^+ and m-NO_3^-, and (c) NO_2^- and b-NO_3^- species on TiO_2 as a function of time.

Fig. 5. Temporal evolution of normalized absorbance of adsorbed N_2O_4 species on TiO_2 surface, for partial pressures 25 and 100 Pa, as a function of time.

Fig. 6. Temporal evolution of normalized absorbances of (a) m-NO_3^- and (b) NO^+ species for various partial pressures as a function of time.

Fig. 7. Temporal evolution of normalized absorbance of NO_2^- produced on TiO_2 surface for 25 and 100 Pa partial pressures as a function of time. NO_2 was introduced at room temperature and under dark condition.

Fig. 8. Temporal evolution of normalized absorbance of b-NO_3^- produced on TiO_2 for various NO_2 partial pressures as a function of time.

Table 1. Vibration assignments of adsorbed species produced during NO_2 adsorption on TiO_2 at 296 K.

Adsorbed species	**Wavenumber (cm^{-1})**	
	In this work	**In literature**
N_2O_4	1708, 1360, 1273	1710, 1350-1370, 1270-1265 [17,18]
NO^+	1914, 1858	1910-1890, 1840-1860 [17,28]
NO_2^-	1222	1225-1202 [18]
monodentate NO_3^-	1542 & 1243	1500-1600 [16,17]
bidentate NO_3^-	1608, 1582, 1288	1585-1605, 1280-1292 [25,26]
bridged NO_3^-	1628, 1171	1624-1590, 1200-1150 [27]